J|A|C|S ARTICLES

Published on Web 03/02/2009

Understanding the Molecule−Surface Chemical Coupling in SERS

Seth M. Morton and Lasse Jensen*

The Pennsylvania State University, Department of Chemistry, 104 Chemistry Building, University Park, Pennsylvania 16802

Received November 22, 2008; E-mail: jensen@chem.psu.edu

Abstract: The enhancement mechanism due to the molecule-surface chemical coupling in surface-enhanced Raman scattering (SERS) has been characterized using time-dependent density functional theory. This has been achieved with a systematical study of the chemical enhancement of *meta*- and *para*-substituted pyridines interacting with a small silver cluster (Ag_{20}). Changing the functional groups on pyridine enabled us to modulate the direct chemical interactions between the pyridine ring and the metal cluster. Surprisingly, we find that the enhancement does not increase as more charge is transferred from the pyridine ring to the cluster. Instead, we find that the magnitude of chemical enhancement is governed to a large extent by the energy difference between the highest occupied energy level (HOMO) of the metal and the lowest unoccupied energy level (LUMO) of the molecule. The enhancement scales roughly as $(\omega_X/\bar{\omega}_e)^4$, where $\bar{\omega}_e$ is an average excitation energy between the HOMO of the metal and the LUMO of the molecule and ω_X is the HOMO−LUMO gap of the free molecule. The trend was verified by considering substituted benzenethiols, small molecules, and silver clusters of varying sizes. The results imply that molecules that show significant stabilization of the HOMO−LUMO gaps (such as those that readily accept π-backbonding) would be likely to have strong chemical enhancement. The findings presented here provide the framework for designing new molecules which exhibit high chemical enhancements. However, it remains a challenge to accurately describe the magnitude of the Raman enhancements using electronic structure methods, especially density functional theory, because they often underestimate the energy gap.

Introduction

Raman spectroscopy is a powerful technique for determining structural information about a system, but the small cross section of Raman scattering typically results in low resolution and/or the need for high concentrations of analyte.[1] However, for analytes near rough metal surfaces, the signal can be enhanced by factors as large as $10^{10}-10^{15}$ due to the strong local field arising from the plasmon excitation combined with the direct chemical interactions between the molecule and the metal surface.[1−8] This is known as surface enhanced Raman scattering (SERS) and has potential to be exploited as a single-molecule spectroscopy. In recent years, SERS has been transformed into a powerful analytic technique[6,9−13] due to advances in nanofabrication[14−20] combined with an increased understanding of plasmonic properties of nanomaterials.[21−24]

Since its initial discovery 30 years ago,[2−4] our qualitative understanding of the underlying enhancement has matured and the total enhancement can roughly be understood in terms of four mechanisms:[8,25] an electromagnetic mechanism (EM) due

(1) Campion, A.; Kambhampati, P. *Chem. Soc. Rev.* **1998**, *27*, 241–250.
(2) Fleischman, M.; Hendra, P. J.; McQuillan, A. J. *Chem. Phys. Lett.* **1974**, *26*, 163–166.
(3) Jeanmaire, D. L.; Van Duyne, R. P. *J. Electroanal. Chem.* **1977**, *84*, 1–20.
(4) Albrecht, M. G.; Crieghton, J. A. *J. Am. Chem. Soc.* **1977**, *99*, 5215–5217.
(5) Moskovits, M. *Rev. Mod. Phys.* **1985**, *57*, 783–826.
(6) Kneipp, K.; Kneipp, H.; Itzkan, I.; Dasari, R. R.; Feld, M. S. *Chem. Rev.* **1999**, *99*, 2957–2976.
(7) Link, S.; El-Sayed, M. A. *Annu. Rev. Phys. Chem.* **2003**, *54*, 331–366.
(8) Jensen, L.; Aikens, C. M.; Schatz, G. C. *Chem. Soc. Rev.* **2008**, *37*, 1061–1073.
(9) Yonzon, C. R.; Haynes, C. L.; Zhang, X. Y.; Walsh, J. T., Jr.; Van Duyne, R. P. *Anal. Chem.* **2004**, *76*, 78–85.
(10) Schultz, D. A. *Curr. Opin. Biotechnol.* **2003**, *14*, 13–22.
(11) Cao, Y.-W.; Jin, R.; Mirkin, C. A. *Science* **2002**, *297*, 1536–1540.
(12) Penn, S. G.; He, L.; Natan, M. J. *Curr. Opin. Chem. Biol.* **2003**, *7*, 609–615.
(13) Anker, J. N.; Hall, W. P.; Lyandres, O.; Shah, N. C.; Zhao, J.; Van Duyne, R. P. *Nat. Mater.* **2008**, *7*, 442–453.
(14) Xia, Y. N.; Halas, N. J. *MRS Bull.* **2005**, *30*, 338–344.
(15) Murphy, C. J.; Sau, T. K.; Gole, A. M.; Orendorff, C. J.; Gao, J.; Gou, L.; Hunyadi, S. E.; Li, T. *J. Phys. Chem. B* **2005**, *109*, 13857–13870.
(16) Gates, B. D.; Xu, Q.; Stewart, M.; Ryan, D.; Willson, C. G.; Whitesides, G. M. *Chem. Rev.* **2005**, *105*, 1171–1196.
(17) Zhang, X. Y.; Whitney, A. V.; Zhao, J.; Hicks, E. M.; Van Duyne, R. P. *J. Nanosci. Nanotechnol.* **2006**, *6*, 1920–1934.
(18) Henzie, J.; Barton, J. E.; Stender, C. L.; Odom, T. W. *Acc. Chem. Res.* **2006**, *39*, 249–257.
(19) Jadzinsky, P. D.; Calero, G.; Ackerson, C. J.; Bushnell, D. A.; Kornberg, R. D. *Science* **2007**, *318*, 430–433.
(20) Dieringer, J. A.; Lettan, R. B.; Scheidt, K. A.; VanDuyne, R. P. *J. Am. Chem. Soc.* **2007**, *129*, 16249–16256.
(21) Yang, W.-H.; Schatz, G. C.; Van Duyne, R. P. *J. Chem. Phys.* **1995**, *103*, 869–875.
(22) Kelly, K. L.; Coronado, E. A.; Zhao, L. L.; Schatz, G. C. *J. Phys. Chem. B* **2003**, *107*, 668–677.
(23) Prodan, E.; Radloff, C.; Halas, N. J.; Nordlander, P. *Science* **2003**, *302*, 419–422.
(24) Wang, H.; Brandl, D. W.; Nordlander, P.; Halas, N. J. *Acc. Chem. Res.* **2007**, *40*, 53–62.

10.1021/ja809143c CCC: $40.75

to resonance of the incident beam with the plasmon of the metal surface, a charge transfer (CT) mechanism due to resonance of the incident beam with an excitation from the metal to the adsorbate, a molecular resonance mechanism (resonance) where the incident beam is resonant with a molecular excitation, and an enhancement due to nonresonant interactions between the surface and the adsorbate (CHEM).[1,5,8] It is important to realize that the four mechanisms are not independent of each other, but rather one or more of the four mechanisms will work in concert to give the total enhancement depending on the wavelength used in the experiment and the specific adsorbate and metal. Even though it may not always be possible to separate these different mechanisms experimentally or theoretically, certain limits can be established where one mechanism is dominating. This is evident from the recent work by Lombardi and Birke[25] who presented a unified expression describing SERS based on a Herzberg−Teller expansion of the general expression for a molecule−metal system. This expression contained three resonances arising from the plasmon resonance, metal−molecule CT transition, and the molecular resonance, and illustrates the coupling between the different terms. Far from any resonances in the system, the CHEM enhancement is recovered. It is well accepted that in most cases the strongest enhancement stems from EM,[1,5,26,27] and many studies have been devoted to understanding this mechanism. The CT, resonance, and CHEM mechanisms are often lumped together into a general chemical mechanism (CM) because a clear separation of these effects is challenging.

To isolate the CM enhancement, SERS has been studied for adsorbates on smooth surfaces, which are known to be unable to support large surface plasmons. These studies showed only small (10^1-10^2) enhancements.[28,29] However, recent theoretical[30] and experimental[31,32] findings indicate that under certain conditions the CM enhancement mechanism can be much larger than is usually thought. Also, large SERS enhancements have been observed for molecules interacting with small nanoclusters or nanocrystalline semiconductor surfaces, both of which are not expected to support plasmon resonances and thus should show only small EM enhancement.[33−35] Combined with the fact that rhodamine 6G, the prototypical single-molecule SERS chromophore,[36−39] is resonantly enhanced by as much as 10^6,[40] these observations provide an important motivation for understanding the general CM mechanism. In addition, there is a growing interest in using electronic structure theory and, in particular, time-dependent density functional theory (TD-DFT), to understand the microscopic nature of SERS.[8] Therefore, it becomes increasingly important to understand from first-principles the factors that govern the Raman enhancements.

The theoretical description of the CT mechanism has been considered in great detail using techniques known from resonance Raman scattering. Lombardi et al. used a Herzberg−Teller expansion of the polarizability to account for metal−molecule CT and molecular resonances.[25,41,42] Arenas et al. used a two-state resonance Raman model connecting the ground-state and the CT excited-state to investigate the effect of CT on the relative Raman intensity.[43−45] Quantum chemical calculations of static Raman intensities can provide a measure of the nonresonant chemical (CHEM) enhancements that arise during analyte adsorption onto a metal cluster or surface. Such calculations are particularly useful in describing shifts in the vibrational frequencies of a molecule due to adsorption onto the metal surface. The relative Raman intensities depend sensitively on the size, charge, binding site, and orientation of the cluster with respect to the molecule. Therefore, numerous researchers have examined CHEM effects in SERS by employing small metal clusters and electronic structure methods. Issues that have been considered include the binding geometry of the adsorbate,[46] the effects of adsorption on various noble and transition metal surfaces,[47] the influence of positively charged atoms at the metal surface,[48,49] the effect of coadsorbed chloride anions,[50] the consequences of nonzero static electric fields,[51] and the solvent effects in the calculations.[52] However, there has been no systematic study so far that elucidates the factors that govern the CHEM enhancement by keeping the metal cluster fixed and varying the molecules.

In this article, we will present a systematic study of the CHEM enhancement of pyridine derivatives interacting with a small silver cluster (Ag_{20}) using TD-DFT. To achieve the microscopic insight, we simulated the bonding and Raman properties of a large set of pyridine-derivatives, which only differ in their functional groups in the *para*- and *meta*-positions. By

(25) Lombardi, J. R.; Birke, R. L. *J. Phys. Chem. C* **2008**, *112*, 5605–5617.
(26) Schatz, G. C.; Van Duyne, R. P. Electromagnetic mechanism of surface enhanced spectroscopy. In *Handbook of Vibrational Spectroscopy*; Chalmers, J. M., Griffiths, P. R., Eds.; John Wiley and Sons, Ltd: New York, 2002; Vol. 1, pp 759−774.
(27) Schatz, G. C.; Young, M. A.; Van Duyne, R. P. Electromagnetic mechanism of SERS. In *Topics in Applied Physics*; Kneipp, K., Moskovits, M., Kneipp, H., Eds.; Springer-Verlag: Berlin, Heidelberg, 2006; Vol. 103, pp 19−46.
(28) Udagawa, M.; Chou, C.-C.; Hemminger, J. C.; Ushioda, S. *Phys. Rev. B* **1981**, *23*, 6843.
(29) Jiang, X.; Campion, A. *Chem. Phys. Lett.* **1987**, *140*, 95–100.
(30) Zhao, L. L.; Jensen, L.; Schatz, G. C. *Nano Lett.* **2006**, *6*, 1229–1234.
(31) Nikoobakht, B.; Wang, J.; El-Sayed, M. A. *Chem. Phys. Lett.* **2002**, *366*, 17–23.
(32) Fromm, D. P.; Sundaramurthy, A.; Kinkhabwala, A.; Schuck, P. J.; Kino, G. S.; Moerne, W. E. *J. Chem. Phys.* **2006**, *124*, 061101(1)−061101(4) .
(33) Peyser-Capadona, L.; Zheng, J.; Gonzalez, J. I.; Lee, T.-H.; Patel, S. A.; Dickson, R. M. *Phys. Rev. Lett.* **2005**, *94*, 058301(1)−058301(4) .
(34) Zheng, J.; Ding, Y.; Tian, B.; Wang, Z. L.; Zhuang, X. *J. Am. Chem. Soc.* **2008**, *130*, 10472–10473.
(35) Yang, L.; Jiang, X.; Ruan, W.; Zhao, B.; Xu, W.; Lombardi, J. R. *J. Phys. Chem. C* **2008**, *112*, 20095–20098.
(36) Nie, S. M.; Emory, S. R. *Science* **1997**, *275*, 1102–1106.
(37) Kneipp, K.; Wang, Y.; Kneipp, H.; Perelman, L. T.; Itzkan, I.; Dasari, R. R.; Feld, M. S. *Phys. Rev. Lett.* **1997**, *78*, 1667–1670.
(38) Xu, H.; Bjerneld, E. J.; Käll, M.; Börjesson, L. *Phys. Rev. Lett.* **1999**, *83*, 4357–4360.
(39) Michaels, A. M.; Nirmal, M.; Brus, L. E. *J. Am. Chem. Soc.* **1999**, *121*, 9932–9939.
(40) Jensen, L.; Schatz, G. C. *J. Phys. Chem. A* **2006**, *110*, 5973–5977.
(41) Lombardi, J. R.; Birke, R. L.; Lu, T.; Xu, J. *J. Chem. Phys.* **1986**, *84*, 4174–4180.
(42) Lombardi, J. R.; Birke, R. L. *J. Chem. Phys.* **2007**, *126*, 244709.
(43) Arenas, J. F.; Soto, J.; Pelaez, D.; Fernandez, D. J.; Otero, J. C. *Int. J. Quantum Chem.* **2005**, *104*, 681–694.
(44) Arenas, J. F.; Woolley, M. S.; Otero, J. C.; Marcos, J. I. *J. Phys. Chem.* **1996**, *100*, 3199–3206.
(45) Arenas, J. F.; Tocón, I. L.; Otero, J. C.; Marcos, J. I. *J. Phys. Chem.* **1996**, *100*, 9254–9261.
(46) Vivoni, A.; Birke, R. L.; Foucault, R.; Lombardi, J. R. *J. Phys. Chem. B* **2003**, *107*, 5547–5557.
(47) Wu, D.-Y.; Duan, S.; Ren, B.; Tian, Z.-Q. *J. Raman Spectrosc.* **2005**, *36*, 533–540.
(48) Cardini, G.; Muniz-Miranda, M. *J. Phys. Chem. B* **2002**, *106*, 6875–6880.
(49) Wu, D.-Y.; Ren, B.; Jiang, Y.-X.; Xu, X.; Tian, Z.-Q. *J. Phys. Chem. A* **2002**, *106*, 9042–9052.
(50) Cardini, G.; Muniz-Miranda, M.; Pagliai, M.; Schettino, V. *Theor. Chim. Acta* **2007**, *117*, 451–458.
(51) Johansson, P. *Phys. Chem. Chem. Phys.* **2005**, *7*, 475–482.
(52) Wu, D. Y.; Hayashi, M.; Lin, S. H.; Tian, Z. Q. *Spectrochim. Acta, Part A* **2004**, *60*, 137–146.

simply changing the functional groups on the pyridine, this study allows us to modulate the direct chemical interactions between the pyridine ring and the metal cluster. Surprisingly, we find that the enhancement does not increase as more charge is transferred from the pyridine ring to the cluster. Instead, we find that the magnitude of the CHEM enhancement is, to a large extent, governed by the energy difference between the highest occupied energy (HOMO) level of the metal and the lowest unoccupied energy (LUMO) level of the molecule. The enhancement scales roughly as $(\omega_X/\bar{\omega}_e)^4$ where $\bar{\omega}_e$ is an average excitation energy between the HOMO of the metal and the LUMO of the molecule and ω_X is the HOMO−LUMO gap of the free molecule. Furthermore, to test the generality of the observed trend we also examined the enhancement for pyridine interacting with silver clusters having different sizes, and different adsorbates both chemisorbed (substituted benzenethiols) and physisorbed (CO, N_2, NH_3, PH_3). The enhancements of the different systems were all shown to follow the same trend. The results imply that molecules that show significant stabilization of the HOMO−LUMO gaps (such as those that readily accept π-backbonding) would be likely to have strong CHEM enhancement. The findings presented here provides the framework for designing new molecules which exhibit high CHEM enhancements. However, it remains a challenge to accurately describe the magnitude of the Raman enhancements using electronic structure methods, especially using density functional theory because they often underestimate the energy gap.

Computational Details

All calculations presented in this work were performed using a local version of the Amsterdam Density Functional (ADF) program package.[53,54] The Becke-Perdew (BP86) XC-potential[55,56] and a triple-ζ polarized slater type (TZP) basis set from the ADF basis set library were used. The 1s-3d core was kept frozen for Ag, and all cluster-molecule complexes used frozen 1s cores for C, N, O, and F, frozen 1s-2p cores for S, P, and Cl, frozen 1s-3p cores for Br, and frozen 1s-4p cores for I. The vibrational frequencies and normal modes were calculated within the harmonic approximation, which seems to be appropriate for the pyridine−silver system.[46] For this reason, the BP86 functional has been chosen because it usually gives harmonic frequencies close to experimental results without the use of scaling factors.[57] Additionally, all Ag atoms were frozen in the vibrational frequency calculations to reduce the computational time. This is a reasonable approximation because Ag vibrational frequencies are significantly lower in frequency than that of row 2 and 3 atoms. The cluster geometries for Ag_{20}-Ag_{68} were taken from the work of Doye and Wales[58] and correspond to global minima using the Sutton−Chen potential. Other silver clusters were taken from our previous work.[59,60] For excitation calculations, the lowest 15 symmetry allowed transitions were calculated. Fragment analyses were performed to determine bonding energy.[61]

To calculate the Raman spectra of the isolated molecules (X), full geometry optimizations were performed, followed by a vibrational frequency and Raman intensity calculation, using the Response[62] module as implemented in ADF. For the cluster−molecule complexes (X-Ag), full geometry optimization and frequency calculations were performed, and polarizability derivatives were then calculated by numerical three-point differentiation with respect to the normal mode displacements[63] using the AOResponse[64,65] module. This allows us to selectively study the Raman intensities of the normal modes associated with the adsorbed molecules. All polarizability calculations were performed at zero frequency using the Adiabatic Local Density Approximation (ALDA). Absolute Raman intensities are presented here as the differential Raman scattering cross section. For Stokes scattering with an experimental setup of a 90° scattering angle and perpendicular plane-polarized light, the cross section is given by[66]

$$I^k = \frac{d\sigma}{d\Omega} = \frac{\pi^2}{\varepsilon_0^2}(\tilde{\nu}_{in} - \tilde{\nu}_k)^4 \frac{h}{8\pi^2 c\tilde{\nu}_k}\left[45\bar{\alpha}'^2_k + 7\gamma'^2_k\right] \times \frac{1}{45(1 - \exp(-hc\tilde{\nu}_k/k_B T))} \quad (1)$$

where $\tilde{\nu}_{in}$ and $\tilde{\nu}_k$ are the frequency of the incident light and of the k^{th} vibrational mode, respectively. $\bar{\alpha}'_k$ and γ'_k are the isotropic and anisotropic polarizability derivatives with respect to the vibrational mode k. We used a wavelength of 512.15 nm (sodium D line) in eq 1 to calculate the Raman cross sections.

To consistently compare the enhancement between the different molecules, we chose to quantify it in terms of the integrated Raman enhancement, defined as the ratio of the total Raman cross section of the complex, I^{tot}_{X-Ag}, and the total cross section of the free molecule, I^{tot}_X. The integrated Raman enhancement is then given by

$$EF_{int} = \frac{I^{tot}_{X-Ag}}{I^{tot}_X} = \frac{\sum_k I^k_{X-Ag}}{\sum_j I^j_X} \quad (2)$$

where I^k_{X-Ag} is the differential Raman cross section of the k^{th} normal mode for the complex, and I^j_X is the differential Raman cross section of the j^{th} normal mode for the free molecule. In this way we minimize the variations in specific modes as well as account for differences in the total number of modes of the individual molecules.

Results and Discussion

To elucidate the nature of the ground-state chemical (CHEM) enhancement, we systematically investigated the bonding and Raman properties of a large series of para- and meta-substituted pyridines interacting with a Ag_{20} cluster (X−Ag). Similar to most previous studies, we assume that pyridine binds to the silver cluster through the nitrogen atom in a perpendicular manner (see Figure 1 for an illustration of the complexes with the position of the functional group indicated). Because we are only interested in modulating the direct electronic interactions between the molecule and the metal cluster, we change only the functional groups and keep everything else the same. Only

(53) ADF, http://www.scm.com, 2005.
(54) te Velde, G.; Bickelhaupt, F. M.; Baerends, E. J.; Fonseca Guerra, C.; van Gisbergen, S. J. A.; Snijders, J. G.; Ziegler, T. *J. Comput. Chem.* **2001**, *22*, 931.
(55) Becke, A. D. *Phys. Rev. A* **1988**, *38*, 3098.
(56) Perdew, J. P. *Phys. Rev. B* **1986**, *33*, 8822.
(57) Neugebauer, J.; Hess, B. A. *J. Chem. Phys.* **2003**, *118*, 7215–7225.
(58) Doye, J. P. K.; Wales, D. J. *New J. Chem.* **1998**, *22*, 733–744.
(59) Zhao, L. L.; Jensen, L.; Schatz, G. C. *J. Am. Chem. Soc.* **2006**, *128*, 2911–2919.
(60) Jensen, L.; Zhao, L. L.; Schatz, G. C. *J. Phys. Chem. C* **2007**, *111*, 4756–4764.
(61) Bickelhaupt, F. M.; Baerends, E. J. Kohn−Sham density functional theory: Predicting and understanding chemistry. In *Reviews in Computational Chemistry*; Lipkowitz, K. B., Boyud, B., Eds.; Wiley-VCH: New York, 2000; Vol. 15, pp 1−86.
(62) van Gisbergen, S. J. A.; Snijders, J. G.; Baerends, E. J. *Comput. Phys. Commun.* **1999**, *118*, 119.
(63) Reiher, M.; Neugebauer, J.; Hess, B. A. *Z. Phys. Chem.* **2003**, *217*, 91–103.
(64) Jensen, L.; Autschbach, J.; Schatz, G. C. *J. Chem. Phys.* **2005**, *122*, 224115.
(65) Jensen, L.; Zhao, L. L.; Autschbach, J.; Schatz, G. C. *J. Chem. Phys.* **2005**, *123*, 174110.
(66) Neugebauer, J.; Reiher, M.; Kind, C.; Hess, B. A. *J. Comput. Chem.* **2002**, *23*, 895–910.

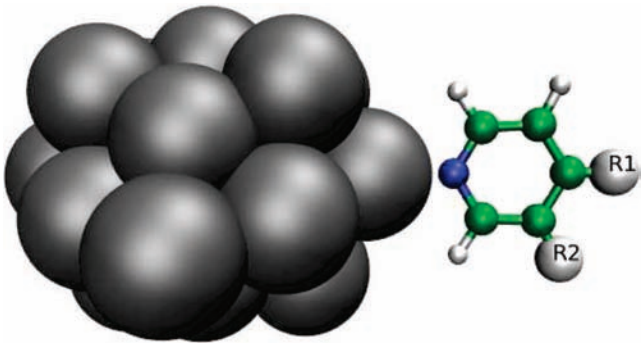

Figure 1. Configurations of the substituted pyridine−Ag_{20} complexes. R1 and R2 indicate the position of functional group in the *para*- and *meta*-substituted pyridines, respectively. Figure was prepared using VMD.[67]

Table 1. Charge Transfer (q(X→Ag)), Bond Length (R_{Ag-N}), Averaged HOMO−LUMO Gap for Complex ($\bar{\omega}_{X-Ag}$), HOMO−LUMO Gap of Free Molecule (ω_X), and Integrated Raman Enhancement (EF_{int}) for Each of the Substituted Pyridines[a]

functional group	q(X→Ag)	R_{Ag-N} (pm)	$\bar{\omega}_{X-Ag}$ (eV)	ω_X (eV)	EF_{int}
p-C≡N	0.040e	224.9	0.077	3.500	81.47
p-CO_2H	0.060e	224.9	0.084	3.265	218.58
p-SO_3H	0.078e	225.7	0.106	3.653	1001.30
m-C≡N	0.093e	227.7	0.123	3.757	1135.62
p-CCl_3	0.104e	226.3	0.161	3.580	4832.51
m-SO_3H	0.113e	227.3	0.177	3.861	4871.75
p-CCl_2H	0.128e	226.4	0.194	3.678	7260.90
p-CFClH	0.130e	226.4	0.229	3.709	7491.35
p-CF_2H	0.130e	226.3	0.235	3.851	7055.83
m-Cl	0.138e	227.1	0.432	4.129	523.44
p-$CClH_2$	0.143e	226.5	0.329	3.741	2091.28
p-I	0.143e	226.3	0.482	4.119	336.73
p-Br	0.144e	227.0	0.487	4.172	317.82
p-Cl	0.145e	226.3	0.472	4.188	293.60
p-F	0.146e	226.5	0.706	4.028	30.27
H	0.151e	226.3	0.633	4.138	52.32
m-OH	0.151e	226.3	0.630	4.065	46.15
p-OH	0.158e	225.9	1.104	4.468	8.98
m-NH_2	0.161e	226.2	0.835	3.756	9.14
p-CH_3	0.163e	225.9	0.802	4.210	17.98
p-NH_2	0.168e	224.5	1.227	4.082	6.74
p-$N(CH_3)_2$	0.181e	223.7	1.420	4.009	5.77

[a] *m*- or *p*- denote the *meta* or *para*-position, respectively. Functional groups listed above H are classified as accepting and below H are classified as donating.

pyridines substituted in the *para*- and *meta*-positions were considered because pyridines substituted in the *ortho*-position will introduce steric hindrance. Functional groups were chosen to give a wide range of partial charge transfer, q(X→Ag), from the molecule to the cluster, and this quantity is used to classify the functional groups as either donating or accepting relative to hydrogen. Table 1 lists q(X→Ag) for each molecule studied. The amount of charge transfer was obtained by calculating the Voronoi deformation density (VDD) charges,[54] which correspond to how much electronic charge enters or leaves a region of space around the nucleus due to the redistribution of charge density from forming the complexes. Thus, any change in the Raman properties of the substituted pyridines must be related to the direct chemical interactions between the molecule and the cluster.

Ag−N Bond Length. A detailed analysis of binding energy and Ag−N bond length (R_{Ag-N}) variations in the complexes was performed to examine the effects of the electronic structure of the complex on the cluster−molecule chemical coupling. The bond lengths for the different complexes are collected in Table 1. For each complex, the bonding energy between the substituted pyridine and the silver cluster is analyzed using the extended transition state method developed by Ziegler and Rauk.[61,68−70] The interaction energy can be decomposed into three physical contributions as[61] $\Delta E = \Delta E^{el} + \Delta E^{Pauli} + \Delta E^{orb}$. The first term is the classical electrostatic interaction between the unperturbed charge distributions of the two fragments, the second term is the Pauli repulsion, which represents the destabilization due to interaction between occupied orbitals and accounts for steric repulsion, and the last term is the interaction between occupied and virtual orbitals and accounts for electron pair bond formation, charge transfer, and polarization.[54] We neglect the preparation energy, that is, the energy needed to deform the isolated fragments to their structure in the complex, and the basis set superposition errors since they were found previously to be rather small (<1 kcal mol^{-1}) for similar systems.[59]

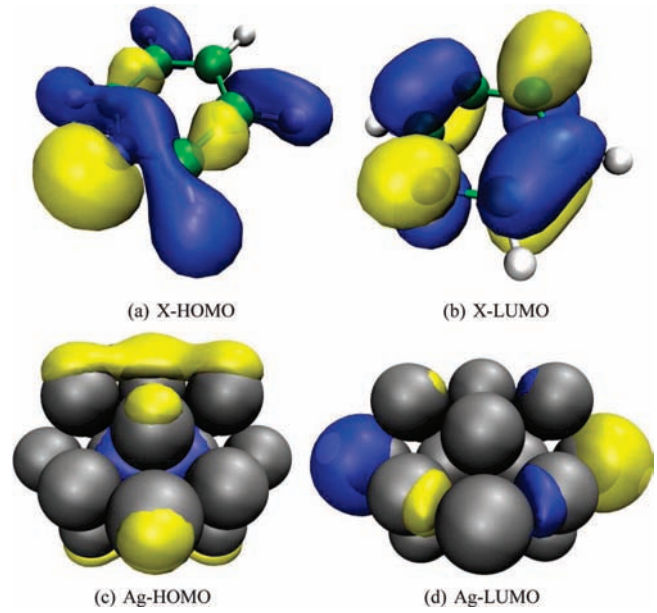

Figure 2. Illustration of the HOMO (X-HOMO) and LUMO (X-LUMO) of pyridine and the HOMO (Ag-HOMO) and LUMO (Ag-LUMO) of the Ag_{20} cluster. Figure was prepared using VMD.[67]

The bonding between the substituted pyridines and the silver cluster is dominated by σ-bonding between the nitrogen atom and the sliver atom with a small contribution from π-back-bonding. X-HOMO and X-LUMO, the orbitals in the substituted pyridines responsible for bonding, are depicted in Figure 2 for the unsubstituted pyridine together with the Ag-HOMO and Ag-LUMO orbitals for the silver cluster. A simplified orbital energy diagram depicting the σ-bonding and π-back-bonding orbitals is shown in Figure 3. As illustrated by the dotted line in Figure 3, σ-bonding occurs primarily through X-HOMO of the substituted pyridines and Ag-LUMO. The dashed line in Figure 3 shows that π-back-bonding occurs through X-LUMO of the pyridine and Ag-HOMO. In fact, about one-third of the total orbital interaction energies (ΔE^{orb}) stem from interactions between these four orbitals (For more detail, please see

(67) Humphrey, W.; Dalke, A.; Schulten, K. *J. Mol. Graph.* **1996**, *14*, 33–38.
(68) Zeigler, T.; Rauk, A. *Theor. Chim. Acta* **1977**, *46*, 1–10.
(69) Ziegler, T.; Rauk, A. *Inorg. Chem.* **1979**, *18*, 1558–1565.
(70) Ziegler, T.; Rauk, A. *Inorg. Chem.* **1979**, *18*, 1755–1759.

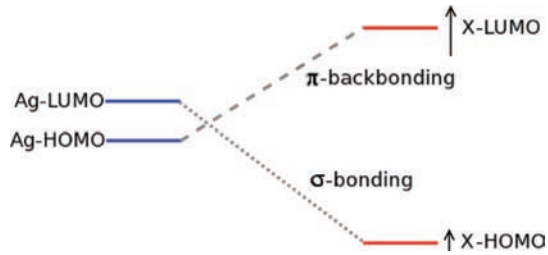

Figure 3. Schematic of the four-orbital bonding model between X and Ag cluster. The dotted line indicates the orbitals primarily responsible for σ-bonding, and the dashed line indicates the orbitals primarily responsible for π-back-bonding. The arrows indicate the direction that the orbitals move as the functional group goes from accepting (A) to donating (D).

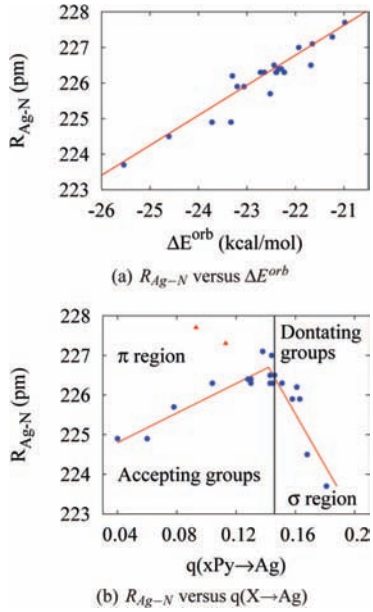

Figure 4. (a) Plot of Ag−N bond length versus orbital interaction energy. (b) Plot of variation in Ag−N bond length versus charge transfer. Red triangles indicate molecules that are bonded through a different orbital and is discussed in Supporting Information. The vertical line marks the unsubstituted pyridine reference, and the other lines are a guide to the eye.

Supporting Information). Increasing the donating character of the functional group raises the energy of both X-LUMO and X-HOMO of the molecule, whereas increasing the accepting character mainly lowers the energy of X-LUMO and only slightly X-HOMO (demonstrated in Figure 3). The Ag-HOMO and Ag-LUMO energy levels of the metal remain almost constant among the different functional groups. Therefore, the effect of the donating groups is to decrease the π-back-bonding by raising the energy of X-LUMO and to increase the σ-bonding by raising the energy of X-HOMO. For the acceptor groups the opposite is true, where the π-back-bonding is increased due to lower X-LUMO and σ-bonding is decreased due to the lowering of X-HOMO.

In Figure 4a, which is a plot of the bond length (R_{Ag-N}) against the orbital interaction energy (ΔE_{orb}), we see that R_{Ag-N} is directly proportional to ΔE^{orb}, which is dominated by the σ- and π-interactions described above. Thus, the bond length is determined by the concerted effects of the σ-bonding and π-back-bonding on ΔE^{orb}. We see that the shortest R_{Ag-N} corresponds to the system with the strongest ΔE^{orb}.

This fact is also reflected in the amount of charge transferred from the molecule to the cluster. To illustrate this, we plot in Figure 4b the bond length as a function of the charge transfer. We find that the bond length relative to pyridine decreased for both acceptor and donor groups. For acceptor groups, less charge is transferred because σ-donation is reduced and π-acceptance is increased, whereas for the donor groups, the opposite effect causes the charge transfer to increase. However, the bond length decreases in both cases because it is governed by the combination of these two effects. As donating character increases, the strength of the σ-bonding increases and compensates for weakening π-back-bonding, shortening R_{Ag-N}. Likewise, as accepting character increases, the π-back-bonding strength increases, which compensates for weakening σ-bonding ans also shortens R_{Ag-N}. Note that R_{Ag-N} decreases slower in Figure 4b for accepting groups than for donating groups; this is because π-back-bonding is a weaker effect than σ-bonding.

CHEM Enhancement. To establish the effects that govern the CHEM enhancement in SERS, we simulated the Raman spectra for the substituted pyridines alone and for the cluster-molecule complexes. All calculations were done in the static limit to ensure that there was no contribution from resonance of the exciting wavelength with CT excitations or surface plasmons. Therefore, any enhancement of the Raman cross sections is solely due to the direct cluster−molecule chemical coupling and should reflect the CHEM enhancement mechanism described in the introduction.

In Figure 5 we present the normal Raman spectrum of pyridine, the Raman spectrum of the pyridine−Ag_{20} complex as well as the Raman spectra of a strong acceptor-substituted complex (CHFCl-Py-Ag_{20}) and a strong donor-substituted complex ($N(CH_3)_2$-Py-Ag_{20}). The Raman intensity of the pyridine molecule is characteristic of all the substituted pyridines. We see that the Raman cross section of pyridine is enhanced by around a factor of 50 when absorbed onto the metal cluster, which is higher than our previous results of pyridine interacting with a tetrahedral Ag_{20} cluster.[59,60] This merely reflects the dependence of the Raman scattering on the geometry of the metal and is the reason we do not change the silver cluster for the substituted pyridine data set. We also see that the Raman cross section for the strong acceptor-substituted pyridine is enhanced by around a factor of 7500, whereas the Raman cross section of the strong donor-substituted pyridine is only enhanced by a factor of 6. Thus, small changes in the electronic structure of the pyridine greatly affect the interactions between the molecule and the silver cluster. Correspondingly, the enhancement factors vary over three orders of magnitude, which is in good agreement with the expected range based on experimental evidence. From Figure 5 it is also clear that there is a significant variation in the Raman spectra in the fingerprint region between 500−1800 cm^{-1} of the different molecules. However, the ring breathing mode around 1000 cm^{-1} and the ring stretching modes around 1200 and 1600 cm^{-1} are consistently enhanced among the different molecule. This is not surprising because they all contain motion toward the silver cluster without significant motion of the functionalized carbon atom.

To compare the Raman enhancements for the different molecules, we calculated the integrated enhancement, EF_{int} in eq 2, by including all modes in the region from ~500 to ~1800 cm^{-1}. The variation among I_X^{tot} for the different pyridine molecules was found to be small ($2.3 \times 10^{-35} \pm 0.7 \times 10^{-35}$ cm^2/sr). This means that the differences in EF_{int} mainly reflect variations in I_{X-Ag}^{tot} and, thus, are indicative of differences in how the molecules chemically interact with the silver cluster. We have collected the integrated enhancements for the different

pyridine molecules in Table 1. We see that by simply modifying the functional groups on the pyridine, the CHEM enhancement can be tuned over a range of three orders in magnitude.

To explain the large range of possible enhancements among the very similar molecules, we considered several properties that could be expected to influence the enhancement, such as R_{Ag-N}, ΔE, and $q(X\rightarrow Ag)$. The plots of EF_{int} as a function of these quantities are presented in Supporting Information. It has been shown experimentally that the distance dependence in SERS follows $EF \approx ((a)/(a + R))^{-10}$, where a is the radius of curvature of the roughness feature and R is the distance from the surface.[60] Similarly, it was shown theoretically for pyridine interacting with small metal clusters that the EM enhancement roughly scales as $|E^{loc}|^4 \approx (1)/(R^9)$, with R being the distance from the center of the cluster to the nitrogen atom.[60] Thus, it is reasonable to assume that the CHEM enhancement would also increase as the bond length between the molecule and the surface decreased. However, our data shows clearly that this is not the case. In fact, the molecule with the smallest EF_{int} has the shortest R_{Ag-N} of the systems studied. This also means that the magnitude of the CHEM enhancements does not follow ΔE^{orb}, because it is directly related to R_{Ag-N} (see Figure 4a). Similar results are found for EF_{int} against ΔE, ΔE^{Pauli}, and ΔE^{el}, as can be seen in Supporting Information. However, probably the most interesting result is that the EF_{int} does not increase as more charge is transferred from the molecule to the metal cluster. In fact, as shown in Table 1 we see that the EF_{int} decreases as $q(X\rightarrow Ag)$ increases. This finding is surprising since one would intuitively expect a stronger chemical interaction between the two systems as more charge is donated from the molecule to the cluster.

Two-State Approximation for the CHEM Enhancement. To understand how the changes in the polarizability are related to the changes in the Raman scattering, we partition the total polarizability of the complex into three components as

$$\alpha^{tot} = \alpha^{Ag} + \alpha^{X_c} + \alpha^{X-Ag} \quad (3)$$

where α^{tot} is the total static polarizability of the complex, α^{Ag} is polarizability that belongs to the cluster, α^{X_c} is the polarizability that belongs to the molecule, and α^{X-Ag} is the polarizability that depends on both the molecule and the cluster. The superscript X_c in α^{X_c} is used to differentiate the polarizability in the complex due to molecule−molecule transitions from α^X, the polarizability of the free molecule. It is important to realize that α^{Ag} and α^{X_c} are not simply the polarizability of the isolated fragments, but include the perturbation caused by the complexation. In the static limit, the total polarizability can be written in the sum-over-states formula as

$$\alpha^{tot}_{\alpha\beta} = 2\sum_{i}^{mol}\frac{\mu_{0i,\alpha}\mu_{i0,\beta}}{\omega_{i0}} + 2\sum_{i}^{cluster}\frac{\mu_{0i,\alpha}\mu_{i0,\beta}}{\omega_{i0}} + 2\sum_{i}^{mixed}\frac{\mu_{0i,\alpha}\mu_{i0,\beta}}{\omega_{i0}} \quad (4)$$

where ω_{i0} is the excitation energy and $\mu_{0i,\alpha}$ is the α Cartesian coordinate of the electric transition dipole moment for the excitation from the ground state to some excited state i. The summation in the first term is restricted to the molecules, and the second term belongs to the silver cluster. The last term corresponds to all metal-to-molecule and molecule-to-metal electronic transitions, that is, it contains all CT excitation between the molecule and the silver cluster.

To understand their importance to the Raman enhancement, we need to consider how the above polarizabilities change when the molecule vibrates. Since only the molecule vibrates, it is reasonable to assume that α^{Ag} will only change slightly. Therefore, we expect most of the variation in enhancement to stem from either α^{X_c} or the mixed term α^{X-Ag}. As we found from the energy analysis, the main effect of the different functional groups is to modulate the levels of X-LUMO and X-HOMO, and through them change the interactions between

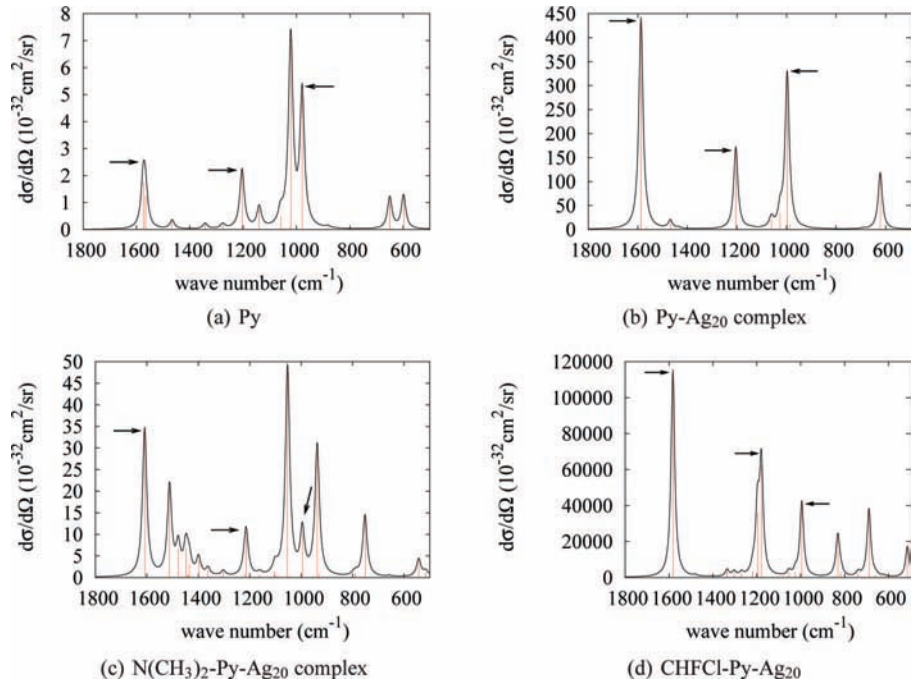

Figure 5. Simulated normal Raman spectra of (a) free pyridine (Py), (b) Py-Ag_{20} complex, (c) $N(CH_3)_2$-Py-Ag_{20} complex, and (d) CHFCl-Py-Ag_{20} complex. Arrows indicate modes strongly enhanced in all systems. Differential cross section in units 10^{-32} cm^2/sr and wavenumber in cm^{-1}. Spectra have been broadened by a Lorentzian having a width of 20 cm^{-1}.

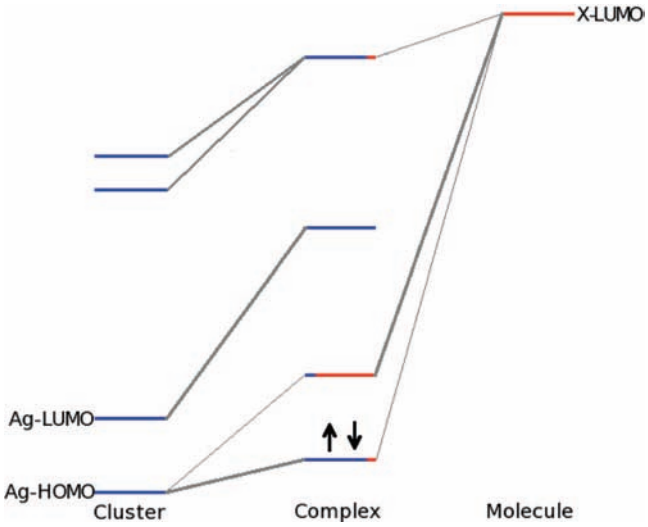

Figure 6. (color online) Schematic of the orbital interaction diagram for the complexes. Lines indicate how the orbitals mix upon complexation. Red represents contributions from the molecule, and blue represents contributions from the cluster.

the molecule and the HOMO and LUMO of the cluster (Ag-HOMO and Ag-LUMO). Therefore, if the mixed polarizability is mainly due to the interactions between these orbitals, we only need to consider the lowest CT transition, ω_e. If we assume such a two-state model, the polarizability derivative for the k^{th} normal mode, Q_k, is then given as[8,65]

$$\frac{\partial \alpha_{\alpha\beta}^{X-Ag}}{\partial Q_k} = -\frac{\mu_{e,\alpha}\mu_{e,\beta}}{\omega_e^2}\left(\frac{\partial \omega_e}{\partial Q_k}\right) \tag{5}$$

where the transition dipole moment for the lowest CT transition, $\mu_{e,\alpha}$, is taken to be independent of Q_k. This expression is similar to the expression derived recently by Lombardi and Birke[25] in the static limit, that is, far from any resonances in the system. We can similarly assume such a two state model for the free molecule, yielding the equation $(\partial\alpha_{\alpha\beta}^{X})/(\partial Q_k) = -(\mu_{X,\alpha}\mu_{X,\beta})/(\omega_X^2)((\partial\omega_X)/(\partial Q_k))$, where ω_X is the lowest excitation in the free molecule, and to a good approximation is the X-HOMO−X-LUMO gap. Therefore, in the two-state approximation, the Raman integrated enhancement is proportional to

$$EF_{int}^{model} = \frac{I_{X-Ag}^{tot}}{I_X^{tot}} \propto \frac{\omega_X^4}{\omega_e^4} \times \frac{(\mu_{e,\alpha}\mu_{e,\beta})^2}{(\mu_{X,\alpha}\mu_{X,\beta})^2}\left(\frac{\partial \omega_e}{\partial Q_k}\right)^2\left(\frac{\partial \omega_X}{\partial Q_k}\right)^{-2} = A\frac{\omega_X^4}{\omega_e^4} \tag{6}$$

where all terms except for the excitation energies are collected into the constant A. The reason for this is that we expect the largest variation between the different molecules to be in the excitation energies for the free molecule (ω_X) and the complex (ω_e).

To assess the validity of this two-state approximation in accounting for the differences in Raman intensities between the complexes, we calculated the lowest electronic excitation energies for the complexes. However, it turned out that it was difficult to identify a single excitation that could explain the variation in EF_{int}. This is due to orbital mixing between the frontier orbitals (HOMO and LUMO) of the molecule and the metal cluster as they form the complex. This is illustrated in Figure 6 where a schematic orbital interaction diagram in the region around the HOMO−LUMO gap is shown. As

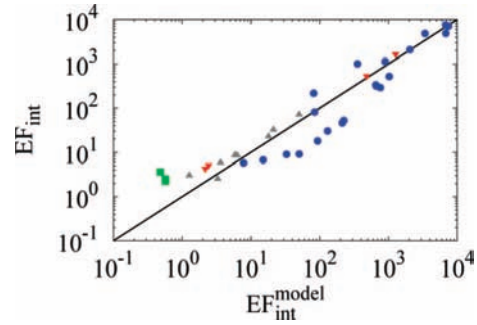

Figure 7. The integrated enhancement, EF_{int}, for each molecule versus the model integrated enhancement, EF_{int}^{model}, calculated using the average two-state model in eq 8 with $A = 0.123$ and $b = 82.93$ eV^{-2}. The blue dots represent the substituted pyridines, the gray pyramids represent the different Ag_n, the red triangles represent the small molecules, and the green squares represent the substituted benzenethiols. The line shown is $y = x$.

illustrated in Figure 6, the main effect is the mixing of Ag-HOMO with X-LUMO; however, some additional mixing occurs as well. The orbital mixing depends strongly on the functional groups whose main effect is to change the energy levels of the frontier orbitals of the molecule relative to the cluster (see Figure 3).

To take into account the differences in the orbital mixing among the different functional groups we considered an average excitation energy defined as

$$\omega_e = \omega_{X-Ag} + \Delta E^{xc} \tag{7}$$

$\bar{\omega}_{X-Ag}$ is the average energy gap between Ag-HOMO and X-LUMO. This is calculated by finding the average energy of the orbitals in the cluster containing X-LUMO, weighted by the percent of X-LUMO in that orbital. The weighted average is also found for Ag-HOMO, and the difference of the two averages gives $\bar{\omega}_{X-Ag}$. ΔE^{xc} is the average contribution to the excitation energy from the exchange-correlation kernel and describes how the orbital energies change when in the excited state. By fitting the difference in the true excitation energy and the average energy gap ($\omega_e - \bar{\omega}_{X-Ag}$) versus $\bar{\omega}_{X-Ag}$, we obtained a functional form describing ΔE^{xc} as $e^{-b\bar{\omega}_{X-Ag}^2}$ (please see Supporting Information). Therefore, our model for EF_{int} in terms of the average excitation energy is given by

$$EF_{int}^{model} \propto A\frac{\omega_X^4}{\bar{\omega}_e^4} = \frac{A\omega_X^4}{\left(\bar{\omega}_{X-Ag} + e^{-b\bar{\omega}_{X-Ag}^2}\right)^4} \tag{8}$$

where we consider A and b as fitting parameters. This average two-state model provides a very good description of the different Raman enhancements as a function of the average energy gap between the metal cluster and the molecule and the X-HOMO-X-LUMO gap of the free molecule by fitting the two parameters A and b. This is illustrated in Figure 7 where we plot the log of EF_{int} for each substituted pyridine (blue dots) versus the log of EF_{int}^{model} obtained from the average two-state model with $A = 0.123$ and $b = 82.93$ eV^{-2}. We see that there is a very good correlation between the model enhancements and the actual enhancements obtained. The variation in the Raman enhancement is thus determined by the ratio of the energy difference between X-HOMO and X-LUMO for the free molecule and Ag-HOMO and X-LUMO in the complex. Since donor groups tend to increase this gap they lower the enhancements, whereas acceptor groups decrease the gap and give higher enhancements.

Table 2. Averaged HOMO−LUMO Gap for Complex ($\bar{\omega}_{X-Ag}$), HOMO−LUMO Gap of Free Molecule (ω_X), and Integrated Raman Enhancement (EF_{int}) for the Three Additional Data Sets Used To Test the Model[a]

system	$\bar{\omega}_{X-Ag}$ (eV)	ω_X (eV)	EF_{int}
	Py-Ag_n		
Ag_6	1.819	4.138	2.54
Ag_8	1.776	4.138	5.83
Ag_{20S}	2.308	4.138	3.01
Ag_{20V}	1.545	4.138	8.47
Ag_{34}	1.141	4.138	32.36
Ag_{40}	0.921	4.138	71.31
Ag_{58}	1.189	4.138	22.61
Ag_{68}	1.576	4.138	8.65
	SM-Ag_{20}		
C≡O	0.888	7.027	531.96
N_2	0.819	8.260	1652.34
NH_3	2.869	6.041	5.11
PH_3	3.180	6.514	4.31
	xBT-Ag_{19}		
p-C≡N	2.359	3.464	2.24
none	2.864	4.027	3.61
p-OH	2.435	3.571	2.51

[a] Py-Ag_n represents the set where the adsorbed molecule (pyridine) was kept the same and the shape and size of the silver cluster was changed. Ag_{20S} and Ag_{20V} represent different bonding locations on the same pyramid shaped cluster, as in reference 59. SM-Ag_{20} represents the set where different small molecules were used as the adsorbate. xBT-Ag_{19} represents the set of *para*-substituted thiolphenols. Please see Supporting Information for representations of these molecules.

To investigate the generality of the proposed model, we also calculated the integrated enhancement for (a) pyridine interacting with silver clusters of different sizes (Ag_n, where n = 6, 8, 34, 40, 58, and 68, and tetrahedal Ag_{20} with pyridine in the S and V conformations from ref 59) where the main effect is due to changes in the Ag-HOMO energy level; (b) small molecules (CO, N_2, NH_3, and PH_3) interacting with the Ag_{20} cluster, which have a significantly different free molecule Raman cross section than pyridine; and (c) three *para*-substituted benzenethiols interacting with a Ag_{19}^+ cluster representing strongly chemisorbed systems. The Ag_{19}^+ cluster was used to ensure a neutral complex since the benzenethiols absorb as thiolates. For these molecules we present in Table 2 the averaged HOMO−LUMO gap for the complex ($\bar{\omega}_{X-Ag}$), the HOMO−LUMO gap of the free molecule (ω_X), and integrated Raman enhancement (EF_{int}). These different systems will probe different aspects of the interactions and thus are a more stringent test of of the model. As clearly seen in Figure 7, the integrated enhancements for these systems are well described using the average two-state model. Note that we did also investigate pyridine interacting with the small clusters Ag_2 and Ag_4, but they gave much lower EF_{int} than predicted from the model. It is therefore likely that these clusters are not adequate for describing SERS due to their small size. We also see from Figure 7 that the minimum enhancements seem to level off around $EF_{int} = 2$. In this region one would expect more states to contribute to the enhancements, explaining why the average two-state model underestimate the enhancements. In general, the EF_{int} of the benzenethiols are much lower than the EF_{int} of the pyridines.

It is important to realized that the CHEM and CT mechanisms have the same origin in the interactions between the metal and the molecule. The CT mechanism[71] stems from a resonance effect caused by an electronic transition between the metal and the LUMO of the molecule. Our results show that the CHEM enhancement is determined by the same charge transfer transition, however, the wavelength of the incident light is off resonance with this transition. In the CT-mechanism, the enhancement scales as $1/\Gamma$,[4] where Γ is the half-width of the electronic transition taken from an absorbance spectrum.[8,42] For metal−molecule CT transitions relevant for SERS, Γ can easily be on the order of 0.5−1 eV. We have shown that for $\Gamma = 0.1$ eV an enhancement of 10^3 can be found; however, it must be considered an upper bound due to the small half-width.[59] The CHEM enhancement scales roughly as $\omega_X^4/\bar{\omega}_c^4$. The results imply that molecules that show significant stabilization of the HOMO−LUMO gaps (such as those that readily accept π-back-bonding) would be likely to have strong CHEM enhancement. This is in good agreement with experimental observations, where aromatic molecules are found to be strongly SERS active. The CT mechanism is often used to explain the dependence of certain bands in SERS experiments on the electrode potential.[43−45] The idea is that by changing the potential, the CT state can be tuned to be at resonance or not. However, our results show that this observation can also be explained by the CHEM mechanism, since changing the potential will modify the position of the Fermi level relative to the molecular levels. Since both mechanisms depend on electronic transitions between the metal and the molecule, we are currently investigating the interplay between these two mechanisms and how the CHEM mechanism depends on the frequency of incident light.

As mentioned in the introduction, there is a growing interest in using electronic structure theory and, in particular TD-DFT, to describe SERS.[8] However, it is well-known that standard TD-DFT calculations underestimate CT excitations in weakly interacting systems and predict the wrong distance dependence.[72] This is related to a deficiency in the adopted exchange-correlations kernel (usually the adiabatic LDA or GGA). The CT excitation energies then become identical to the orbital differences for orbitals with zero overlap. This means that the CHEM enhancements found here are likely to be overestimated. In spite of this, we expect the trend found to be correct, but it will require better functionals if the enhancements are to be calculated more accurately. Several new XC-functionals based on the separation of the Coulomb operator into a long-range part and a short-range part show great promise for correctly describing the CT excitation energies.[73−76] We are therefore currently investigating the importance of such functionals for describing the CHEM enhancements of SERS and providing accurate estimates for the magnitude of the enhancements.

Conclusion

In this study, we have presented a systematic study of the CHEM enhancement of pyridine derivatives interacting with a small silver cluster (Ag_{20}) using TD-DFT. Such small clusters can function as appropriate model systems for obtaining microscopic insights into the SERS enhancement mechanisms. To achieve this microscopic insight, we simulated the bonding

(71) Otto, A.; Futamata, M. In *Electronic Mechanisms of SERS*; KneippK., Moskovits, M., Kneipp, H., Eds.; Springer-Verlag: Berlin, Heidelberg, Germany, 2006; Vol. 103, Chapter 8, pp 147−184.

(72) Dreuw, A.; Weisman, J. L.; Head-Gordon, M. *J. Chem. Phys.* **2003**, *119*, 2943–2946.

(73) Iikura, H.; Tsuneda, T.; Yanai, T.; Hirao, K. *J. Chem. Phys.* **2001**, *115*, 3540–3544.

(74) Vydrov, O. A.; Scuseria, G. E. *J. Chem. Phys.* **2006**, *125*, 234109.

(75) Yanai, T.; Tew, D. P.; Handy, N. C. *Chem. Phys. Lett.* **2004**, *393*, 51–57.

(76) Livshits, E.; Baer, R. *Phys. Chem. Chem. Phys.* **2007**, *9*, 2932–2941.

and Raman properties of a large set of pyridine derivatives that only differ in their functional groups in the *para*- and *meta*-positions. By simply changing the functional groups on the pyridine, this study allowed us to modulate the direct chemical interactions between the pyridine ring and the metal cluster. Surprisingly, we find that the enhancement does not increase as more charge is transferred from the pyridine ring to the cluster. Instead, we find that the magnitude of the CHEM enhancement is, to a large extent, governed by the energy difference between the highest occupied energy level of the metal and the lowest unoccupied energy level of the molecule. The results imply that molecules that show significant stabilization of the HOMO−LUMO gaps (such as those that readily accept π-backbonding) would be likely to have strong CHEM enhancement, which is in good agreement with experimental observations. In addition, because weakly coupled CT excitations are often underestimated using TD-DFT, it remains a challenge to accurately describe the Raman enhancement magnitude using electronic structure methods.

Acknowledgment. L.J. acknowledges start-up funds from the Pennsylvania State University and support received from Research Computing and Cyberinfrastructure, a unit of Information Technology Services at Penn State.

Note Added after ASAP Publication. The version of this paper published on March 2, 2009, contained the wrong Supporting Information file. The version published on March 18, 2009, contains the correct Supporting Information file.

Supporting Information Available: Additional analysis of the bonding properties and Raman enhancement and tables containing optimized geometries. This material is available free of charge via the Internet at http://pubs.acs.org.

JA809143C